RSC Advances

ROYAL SOCIETY OF CHEMISTRY

www.rsc.org/advances

Synthesis of the Visible-Light-Driven $Ag_3VO_4/Ag_3PO_4/Ag$ Photocatalysts with Enhanced Photocatalytic Activity

Elham Akbarzadeh

Department of Chemistry, Sharif University of Technology
Tehran, 11365-11155, Iran

*Shahrbano Rahman Setayesh**

Department of Chemistry, Sharif University of Technology
Tehran, 11365-11155, Iran

*Mohammad Reza Gholami**

Department of Chemistry, Sharif University of Technology
Tehran, 11365-11155, Iran

(*Corresponding author e-mail: Setayesh@sharif.edu)

(*Corresponding author e-mail: gholami@sharif.edu)

Abstract

A novel visible-light-driven $Ag_3VO_4/Ag_3PO_4/Ag$ photocatalyst was successfully synthesized via an anion-exchange reaction and characterized by X-ray diffraction, field emission scanning electron microscopy, X-ray photoelectron spectroscopy, UV-vis diffuse-reflectance spectroscopy and Fourier transform infrared spectroscopy. The photocatalytic activities of prepared catalysts were evaluated by degradation of acid blue 92 (AB92) aqueous solutions under visible light irradiation. The photocatalytic results indicated that the synthesized $Ag_3VO_4/Ag_3PO_4/Ag$ hybrid displays a significantly enhanced activity in degradation of acid blue 92 under visible light compared with pure Ag_3VO_4. The improved photocatalytic activity can be attributed to the efficient separation of photo-induced electrons and holes in the composite. A possible mechanism has been proposed for this improvement.

Keywords: Photocatalyst, $Ag_3VO_4/Ag_3PO_4/Ag$, Degradation, AB92.

1. Introduction

In the past few decades, semiconductor photocatalysis has been widely studied for applications in environmental pollution mediation and solar energy conversion[1-4]. Visible region ($\lambda > 400$ nm) covers the largest proportion of the solar spectrum. In order to transform this technology into practical applications it is essential to develop high-efficiency visible-light-driven photocatalysts. The Ag-based materials have good photocatalytic activity in visible light and hence, they have received much attention as photocatalysts. In recent years, numerous efforts have been devoted to investigate the photocatalytic activity of Ag-based photocatalysts, such as Ag_2CO_3[5], Ag_2O[6], Ag_3PO_4[7] and AgX[8-10] (X=I, Br and Cl). Due to their high visible light sensitivity, facile syntheses and availability of raw materials[11] they have become interesting to researcher. Among them, fabrication of a semiconductor heterojunction by couple of two Ag-based materials is an attractive approach to improve photocatalytic efficiency of them. The AgI/Ag_3PO_4[12], $AgBr/Ag_2CO_3$[13], $Ag_3PO_4/AgBr/Ag$ [14] and $Ag_3VO_4/AgBr/Ag$[15] photocatalysts have been successfully synthesized for toxic chemical degradation. Among this photocatalyst Ag_3VO_4 has become an attractive material after Konta et al.[16] reported its photocatalytic activity under light irradiation. Ag_3VO_4 with a band –gap energy of 2.2 eV[17], is a visible-light-responsive catalyst; however, its photocatalytic activity is limited due to its high recombination rate of photo-induced charge carriers. Therefore, many efforts have been directed towards enhancing its photo-induced electron separation efficiency and improving its photocatalytic activity. For example, $BiOI/Ag_3VO_4$[18], $g\text{-}C_3N_4/Ag_3VO_4$[17]and $ZnFe_2O_4/Ag_3VO_4$[19], have been developed with enhanced photocatalytic efficiency in visible light irradiation compare to the individual photocatalyst.

A novel photocatalyst is introduced by combining Ag_3PO_4, a semiconductor with a band gap of around 2.4 eV[20], with Ag_3VO_4. The $Ag_3VO_4/Ag_3PO_4/Ag$ hybrid synthesized by an anion-exchange reaction and characterized by XRD, FESEM, XPS, DRS and FT-IR spectrometer. The visible-light-response photocatalytic ability of this composite studied by degradation of AB92 in aqueous solution. In addition, photocatalytic mechanism of $Ag_3VO_4/Ag_3PO_4/Ag$ also discussed.

2. Experimental

2. 1 Synthesis of Ag_3VO_4

20 ml solution of NaOH and V_2O_5 with mole ratio of 6:1 was prepared, then 60 ml $AgNO_3$ solution was added dropwise into the above solution under vigorously stirring (Ag/V mole ratio of 3:1).[21] After stirring for 30 min at room temperature, the suspension was transferred into a 200 ml Teflon-lined stainless autoclave and heated for 12 h at 140℃. Finally, the brownish yellow products were collected, washed several times with distilled water and dried in air at 70℃ overnight.

2. 2. Preparation of $Ag_3VO_4/Ag_3PO_4/Ag$ Photocatalyst

$Ag_3VO_4/Ag_3PO_4/Ag$ photocatalysts were prepared through an anion-exchange method in dark condition. 0.1 g of Ag_3VO_4 was dispersed in 20 ml of ethylene glycol. Subsequently, 20 ml of an ethylene glycol solution of NaH_2PO_4 was added drop wise to above solution, after stirring in dark for 40 min, the reaction was continued under visible light for 20 min in order to convert some silver ions on the surfaces of Ag_3VO_4/Ag_3PO_4 to silver nanoparticles. Then, the resulting sample was washed with deionized water and dried in air at 60℃ for 12 h.

2. 3. Characterization of photocatalysts

X-ray diffraction (XRD) analysis of the samples were carried out using a Philips X'pert instrument with a Cu Kα irradiation (λ = 0.15406 nm) at 40 kV/40 mA. Fourier-transform

infrared (FT-IR) spectra were recorded with an ABB BOMER MB series spectrophotometer. The morphologies of the samples were observed using an XL30 Field emission scanning electron microscopy (FESEM). UV-vis diffuse-reflectance spectroscopy (UV-vis DRS) of the obtained samples were done via a GBC Cintra 40 instrument.

2. 4. Evaluation of photocatalytic performance

The photocatalytic activity of the $Ag_3VO_4/Ag_3PO_4/Ag$ was evaluated by decomposition of AB92 under visible light irradiation at the natural pH value. Typically, 0.02 g of catalyst was dispersed in 100 ml of 2.5 gL^{-1} AB92 aqueous solution in a reactor that was surrounded by a running water jacket to keep the temperature unchanged. After stirring in dark for 30 min, to reach the adsorption-desorption equilibrium of AB92 molecules on the surface of catalyst, the suspension was illuminated by a 125 W mercury lamp with a UV cut-off filter as visible light source ($\lambda \geq$ 420 nm). At given time interval (20 min), about 3 mL of the mixture was withdrawn and centrifuged to remove the photocatalyst particles. The photocatalytic degradation process of AB92 was monitored by measuring its characteristic absorption at 571 nm with an UV-vis spectrophotometer.

3. Results and Discussion

3. 1. Characterization of photocatalysts

The crystallographic structure of the as-prepared samples was analyzed by XRD measurements. Figure 1 shows the XRD patterns of Ag_3VO_4 and $Ag_3VO_4/Ag_3PO_4/Ag$ products. All of the diffraction peaks of the Ag_3VO_4 samples can be indexed to the monoclinic phase of Ag_3VO_4 (JCPDS: 43-0542). The composites exhibit several additional peaks which are indexed to Ag_3PO_4 (JCPDS: 06-0505), indicating that Ag_3PO_4 nanocrystals were generated and verifying co-existence of Ag_3VO_4 and Ag_3PO_4 in $Ag_3VO_4/Ag_3PO_4/Ag$ hybrid. However no obvious

characteristic diffraction peaks of Ag^0 species were detected in the $Ag_3VO_4/Ag_3PO_4/Ag$ patterns, because of the low contents of Ag^0.

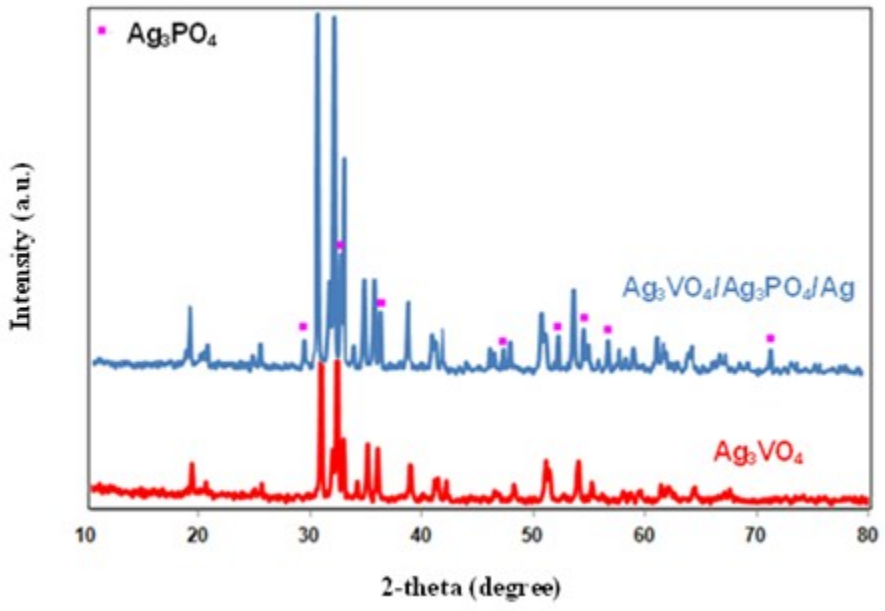

Figure 1. XRD patterns of as prepared Ag_3VO_4 (a) and $Ag_3VO_4/Ag_3PO_4/Ag$ (b) samples.

The microstructures of the samples were obtained by field emission scanning electron microscope. As shown in Figure 2a and b pure Ag_3VO_4 displays irregular polyhedral shapes. It is obvious that the hybrid catalysts (Figure 2c and d) still maintain the morphology and structure of the original shape of Ag_3VO_4 crystals. Figure 2c and d demonstrate that the uniform Ag_3PO_4 covered the surface of Ag_3VO_4 crystals after ion-exchange process. Typical SEM image of $Ag_3VO_4/Ag_3PO_4/Ag$ hybrid (Figure 2e) indicate that some small Ag nanoparticles existed randomly on the surface of Ag_3VO_4/Ag_3PO_4 heterocrystals.

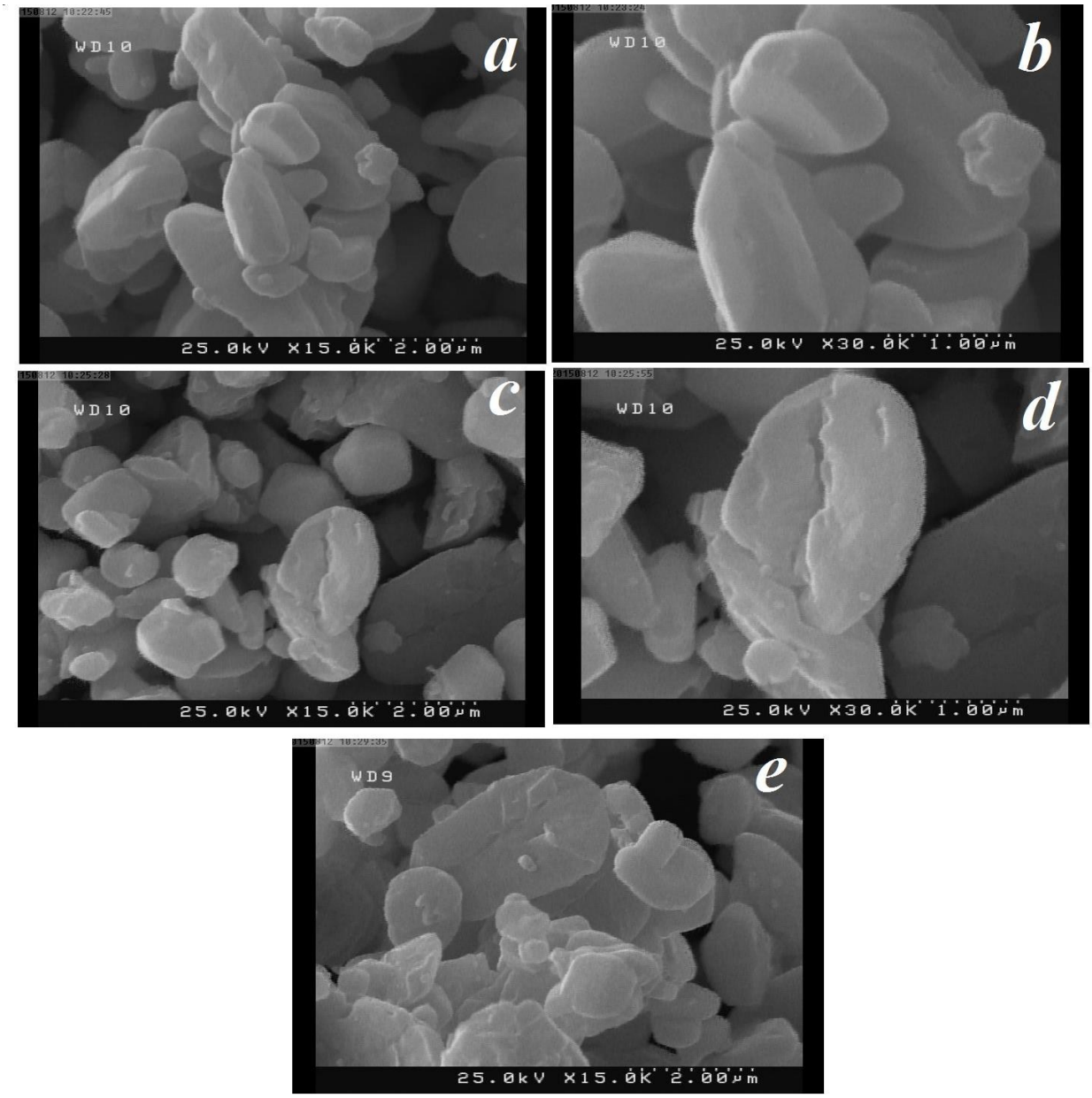

Figure 2. Typical FESEM images of the Ag_3VO_4 (a, b), Ag_3VO_4/Ag_3PO_4 (c, d), and $Ag_3VO_4/Ag_3PO_4/Ag$ (e).

Figure 3 depicts the Fourier transform infrared spectra of $Ag_3VO_4/Ag_3PO_4/Ag$ nanocomposite, pure Ag_3VO_4 and Ag_3PO_4. In FT-IR spectrum of composite, absorption peaks at 740 and 864 cm^{-1} correspond to the stretching vibrations of the VO_4 unit [22]. The peaks at 567 and 1016 cm^{-1}

can be attributed to the stretching vibrations of the PO_4 group[23] which verify the existence of Ag_3PO_4 in the sample, and the peaks around 1600 and 3200 cm^{-1} represent the physically adsorbed water on the catalyst surface.

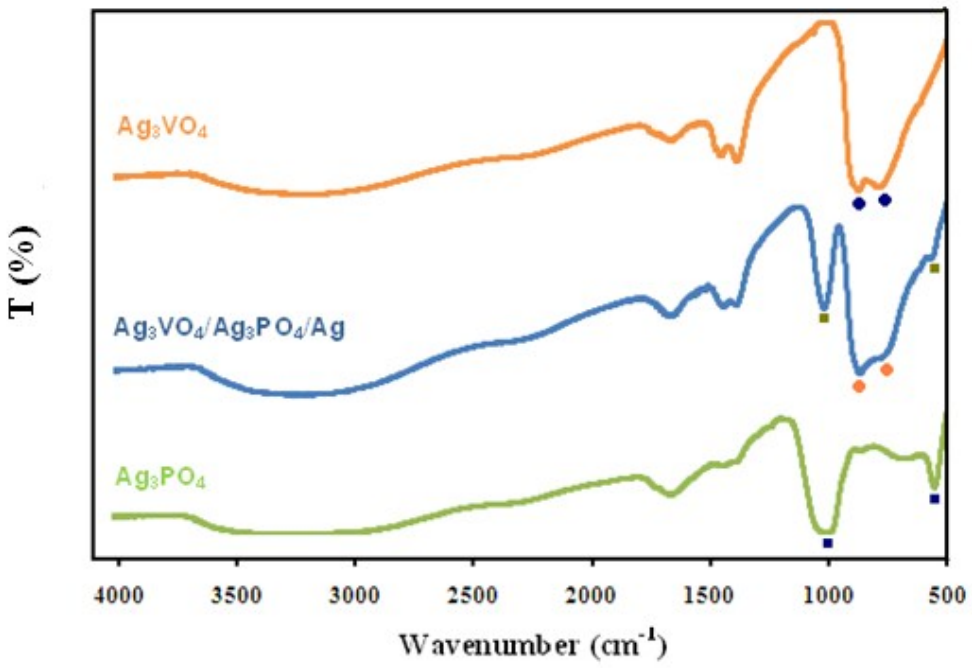

Figure 3. FT-IR spectra of $Ag_3VO_4/Ag_3PO_4/Ag$ composite, pure Ag_3VO_4 and Ag_3PO_4.

To investigate the metallic state of Ag^0 on the surface of photocatalyst, we carried out X-ray photoelectron spectroscopy (XPS), and the results are shown in Figure 4. In the survey spectrum (Figure 4a) the obvious peaks of Ag, C, O, V and P can be clearly detected. The higher resolution XPS data for Ag 3d peaks, shows two individual peaks at approximately 373.1 (Ag $3d_{3/2}$) and 367.1 (Ag $3d_{5/2}$) eV.[24] The Ag $3d_{3/2}$ and Ag $3d_{5/2}$ peaks can be divided into two different bands. The peaks at 373.6 and 367.6 are assigned to Ag^0, and those at 373.1 and 367.1 are attributed to Ag^+ species.[25]

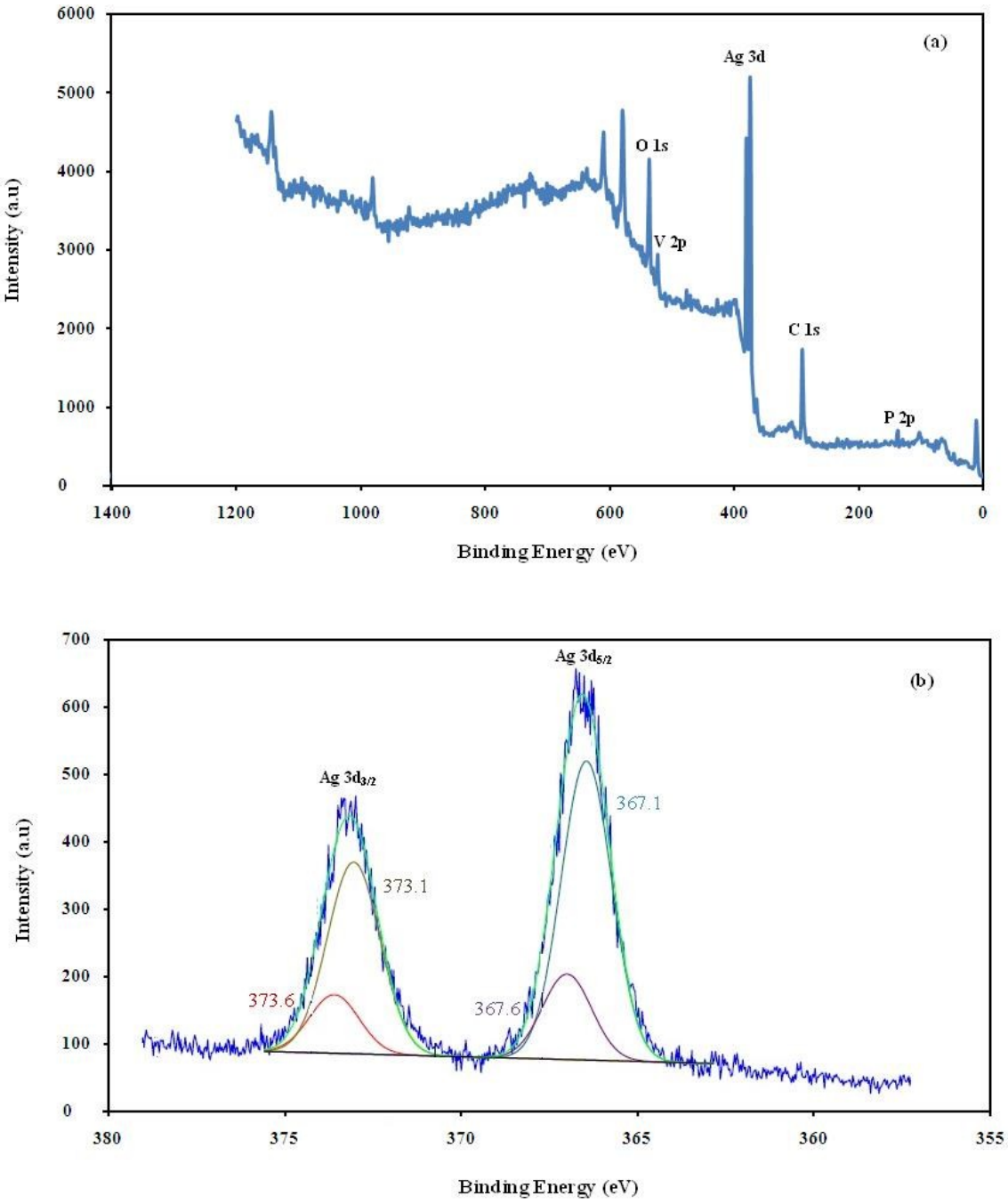

Figure 4. XPS analysis of $Ag_3VO_4/Ag_3PO_4/Ag$: (a) the survey XPS spectrum and (b) the high-resolution spectrum for the Ag 3d states.

The optical response of the $Ag_3VO_4/Ag_3PO_4/Ag$ composite at different light wavelength was determined by UV-vis diffuse reflectance spectroscopy. As seen in Figure 5. Ag_3VO_4 has an adsorption edge at around 610 nm. The $Ag_3VO_4/Ag_3PO_4/Ag$ hybrid displays a much stronger response in visible region than pure Ag_3VO_4 and the visible absorption intensity of the nanocomposite was enhanced, which can attributed to the SPR of the Ag NPs on the surfaces of $Ag_3VO_4/Ag_3PO_4/Ag$[14,15]. Remarkable absorption enhancement leads to good visible light photocatalytic activity.

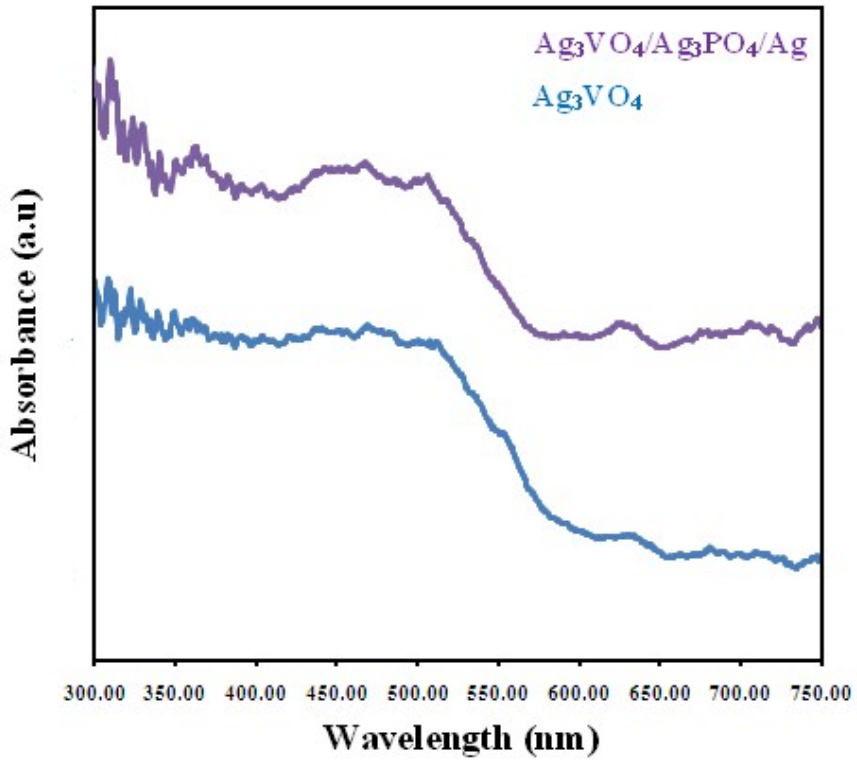

Figure 5. UV-vis diffuse-reflectance spectra of Ag_3VO_4 and $Ag_3VO_4/Ag_3PO_4/Ag$.

3. 2. Photocatalytic Activity of $Ag_3VO_4/Ag_3PO_4/Ag$

The photocatalytic activities of prepared samples for degradation of AB92 were evaluated under visible light irradiation. The photocatalytic degradation efficiency (X%) of AB92 was obtained using formula 1:

$$X\% = \frac{C_0 - C_t}{C_0} \times 100 \quad (1)$$

where C_0 and C_t are the initial concentration and the concentration of AB92 after irradiation for t min, respectively. The degradation efficiency of dye under visible light without the catalyst and with the present of pure Ag_3VO_4, Ag_3VO_4/Ag_3PO_4 and $Ag_3VO_4/Ag_3PO_4/Ag$ hybrid photocatalysts, are shown in Figure 6. It is obvious that in the absence of any catalyst, AB92 is stable while $Ag_3VO_4/Ag_3PO_4/Ag$ hybrid exhibited much higher photocatalytic activity than pure Ag_3VO_4 and Ag_3VO_4/Ag_3PO_4. It can be seen that 84.0% of the AB92 is photocatalytically degraded after 80 min for $Ag_3VO_4/Ag_3PO_4/Ag$ hybrid. Whereas, for the pure Ag_3VO_4 and Ag_3VO_4/Ag_3PO_4 photocatalyst only 22.0% and 76% of AB92 dye molecule is degraded under same condition, respectively.

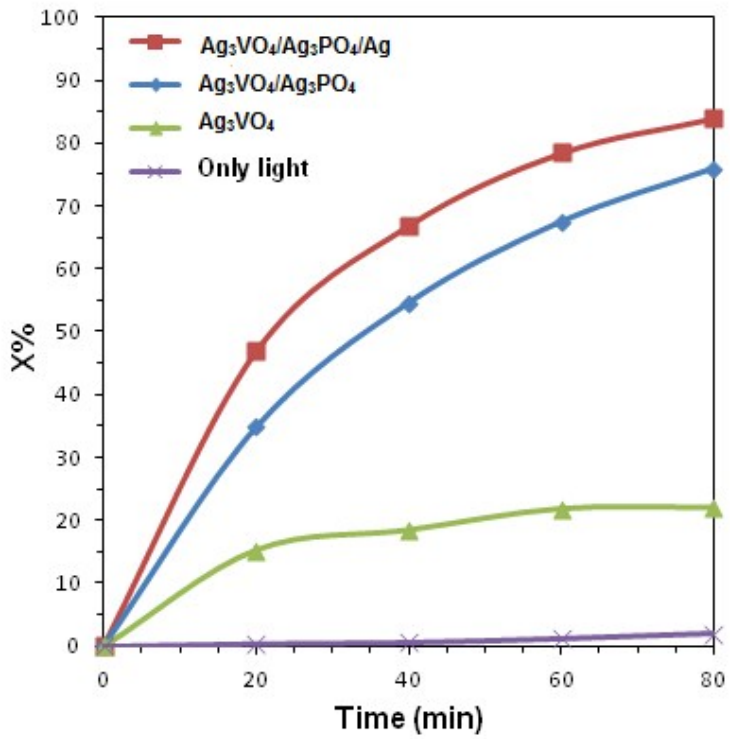

Figure 6. The degradation efficiency of AB92 in the presence of different samples under visible light irradiation.

Linear relationship between $\ln(C_0/C_t)$ and irradiation time, propose that the photocatalytic reaction obeys pseudo-first-order kinetics. The plot of $\ln(C_0/C_t)$ versus t is shown in Figure 7 and according to the Langmuir-Hinshelwood model ($\ln(C_0/C_t) = kt$), the rate coefficient of AB92 degradation over the samples are demonstrated in Figure 8. The photodegradation rate coefficient of $Ag_3VO_4/Ag_3PO_4/Ag$ hybrid (0.022 min^{-1}) is higher by a factor of 11 compare to pure Ag_3VO_4 (0.002 min^{-1}).

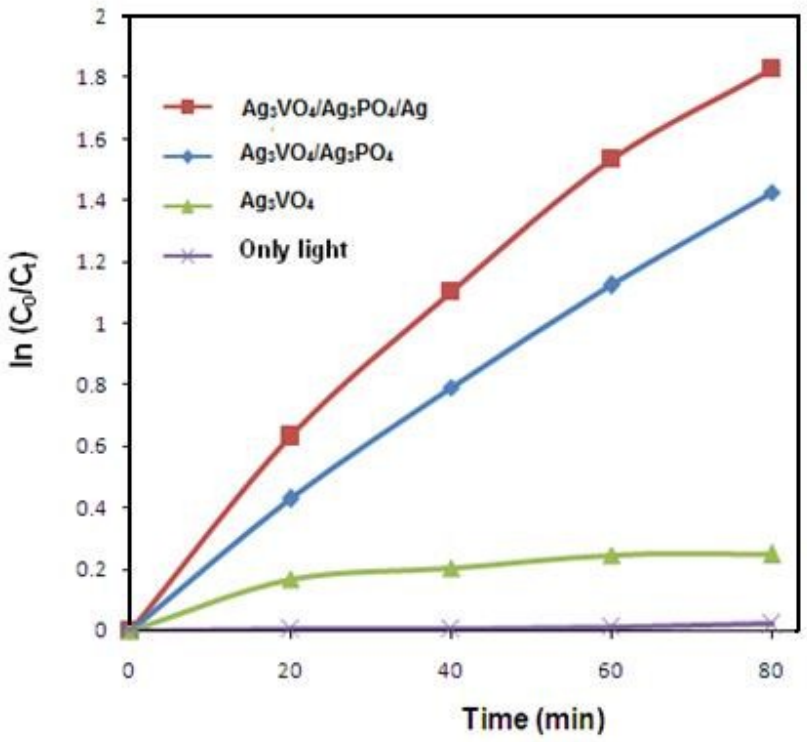

Figure 7. Linear-log plot for AB92 degradation in the presence of as synthesized photocatalysts under visible light illumination.

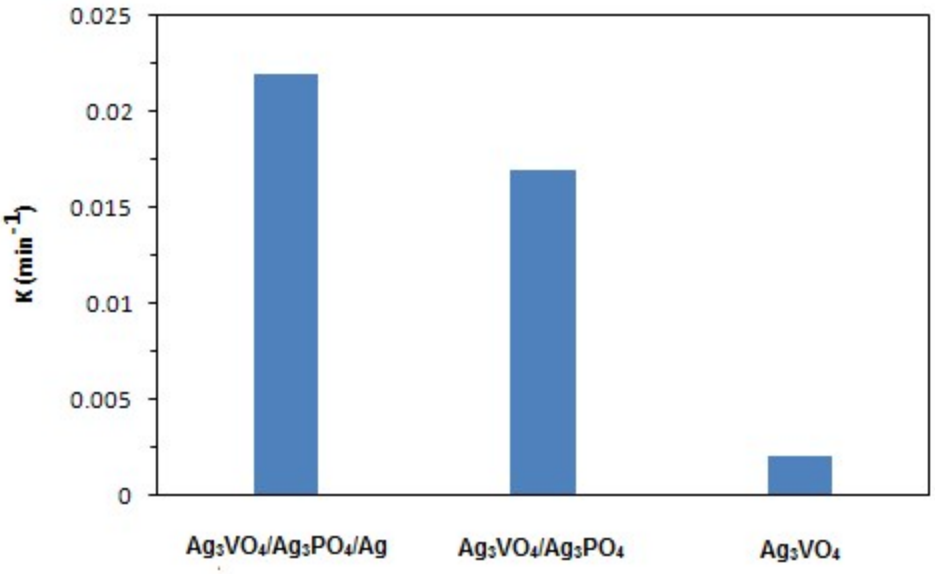

Figure 8. The degradation rate constant under visible light irradiation.

These results clearly indicate that the coupling of Ag_3PO_4 with Ag_3VO_4 greatly enhances the photocatalytic activity which is obvious from changes in UV-visible absorption spectra of AB92 solution at different times using pure Ag_3VO_4 and $Ag_3VO_4/Ag_3PO_4/Ag$ hybrid under visible light. (Figure 9)

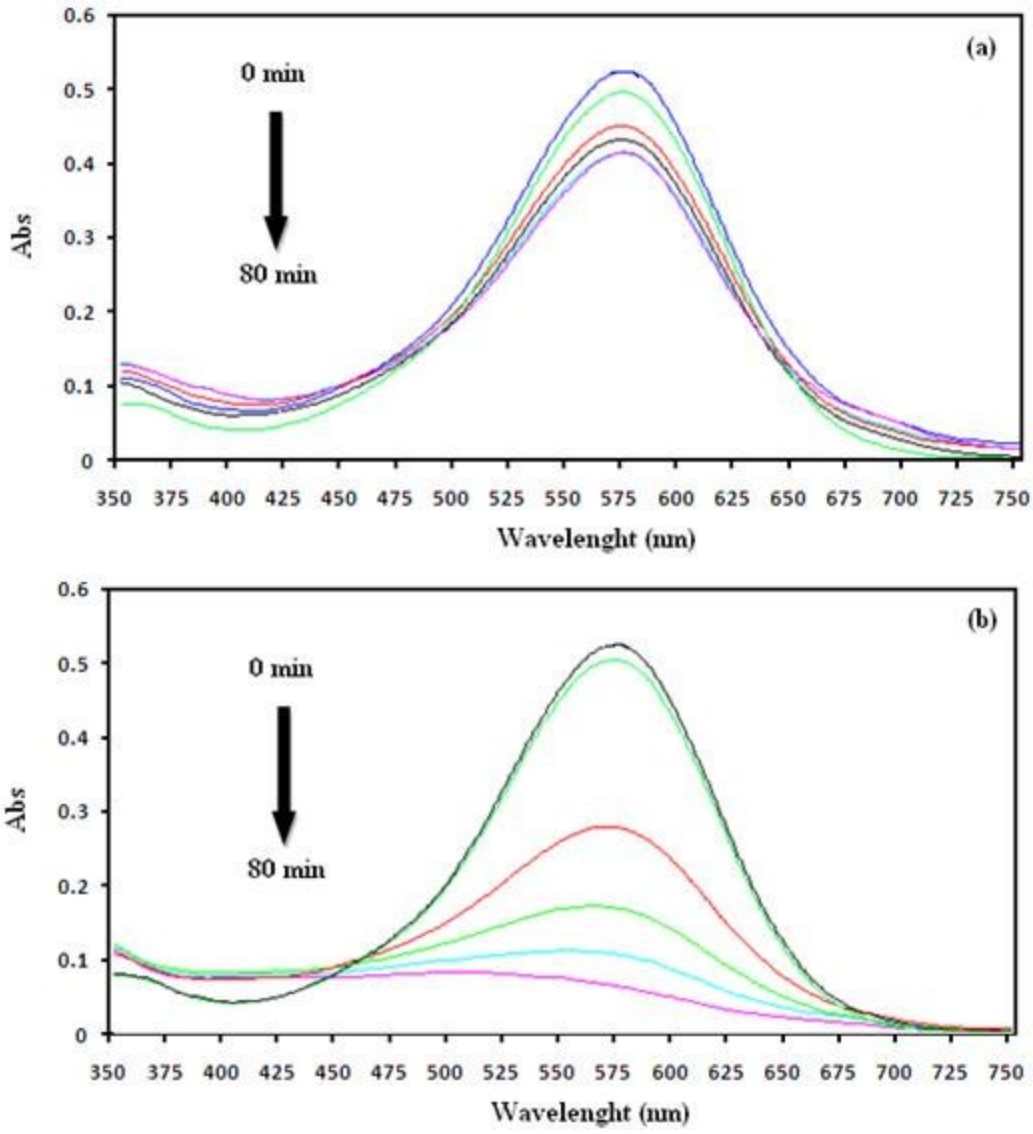

Figure 9. Changes in UV-visible absorption spectra of AB92 solution using pure Ag_3VO_4 (a) and $Ag_3VO_4/Ag_3PO_4/Ag$ (b) hybrid at different times under visible light irradiation.

3.3. Stability of Photocatalyst

Stability of Ag- containing photocatalysts is an important issue for their practical applications. To investigate the stability of $Ag_3VO_4/Ag_3PO_4/Ag$, crystallinity of the fresh and used composite was compared by using XRD patterns. As shown in Figure 10, no obvious crystalline structure changing can be observed in XRD patterns, demonstrating that $Ag_3VO_4/Ag_3PO_4/Ag$

photocatalyst posses high stability. Furthermore the photocatalyst activity after first run was determined about 77%, confirming that $Ag_3VO_4/Ag_3PO_4/Ag$ nanocomposite is stable enough during the photocatalytic process.

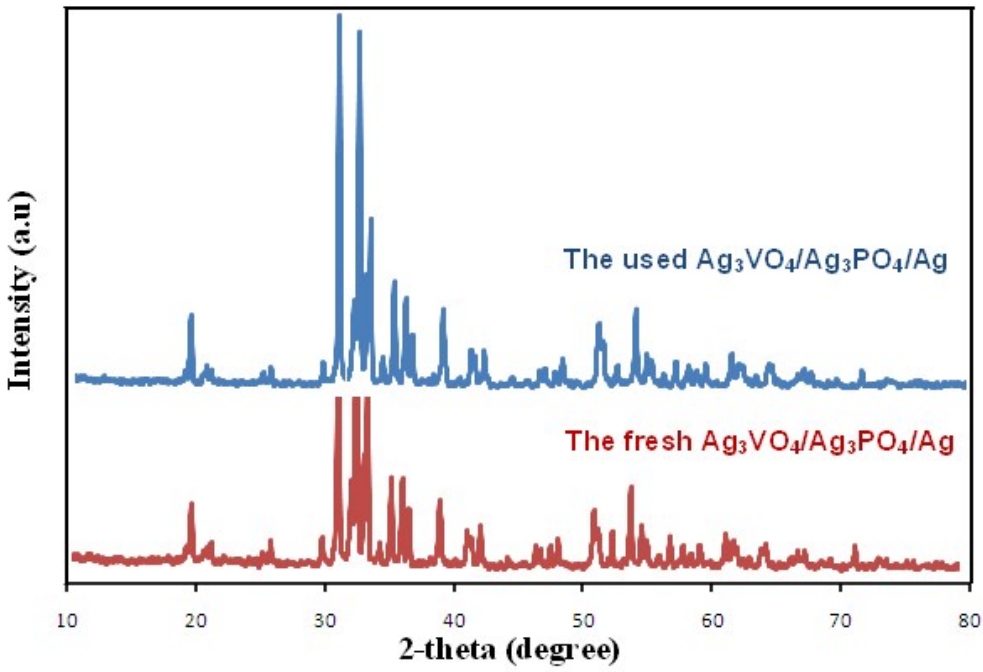

Figure 10. XRD patterns of the $Ag_3VO_4/Ag_3PO_4/Ag$ after photocatalytic experiment.

3.4. Discussion of the Effects of the Reactive Species on the Potodegradation of AB92

It is generally accepted that semiconductor photocatalytic process involves generation of electrons and holes in the conduction band and valance band of semiconductor under light irradiation. Subsequently, in addition to the active hole and electron process, photo-generated charge carriers can react with preadsorbed H_2O/OH^- on the catalyst surface and dissolved oxygen in the solution to produce reactive species [26-28]

$$e_{CB}^- + O_2 \longrightarrow O_2^{\bullet -} \quad (2)$$

$$O_2^{\bullet -} + H^+ \longrightarrow HO_2^{\bullet} \quad (3)$$

$$HO_2^{\bullet} + HO_2^{\bullet} \longrightarrow H_2O_2 \quad (4)$$

$$O_2^{\bullet -} + HO_2^{\bullet} + H^+ \longrightarrow H_2O_2 + O_2 \quad (5)$$

$$h_{VB}^+ + H_2O \longrightarrow OH^{\bullet} \quad (6)$$

$$h_{VB}^+ + OH^- \longrightarrow OH^{\bullet} \quad (7)$$

To consider the effect of these reactive species on the photo degradation of AB92, different scavengers (iodide ion, t-BuOH and p-benzoquinone) were introduced into the AB92 degradation process. As shown in Figure 11, when p-benzoquinone was used as $O_2^{\bullet -}$ scavengers, the degradation of AB92 significantly decreased, demonstrate that molecular oxygen play a major role in the photodegradation of dye molecules. In the present of t-BuOH, the degradation of AB92 remarkably decreased, it can be caused by reaction of t-BuOH with $OH^{\bullet}$ in the solution, this result implying that the $OH^{\bullet}$ play an important role in the reaction. The degradation was almost unchanged in the presence of iodide ion illustrating that h_{VB}^+ and/or surface-adsorbed $OH^{\bullet}$ have very little influence in the degradation of AB92. The above results indicate that both $OH^{\bullet}$ and $O_2^{\bullet -}$ are the predominant reactive species in the photocatalytic degradation of AB92 under visible light irradiation.

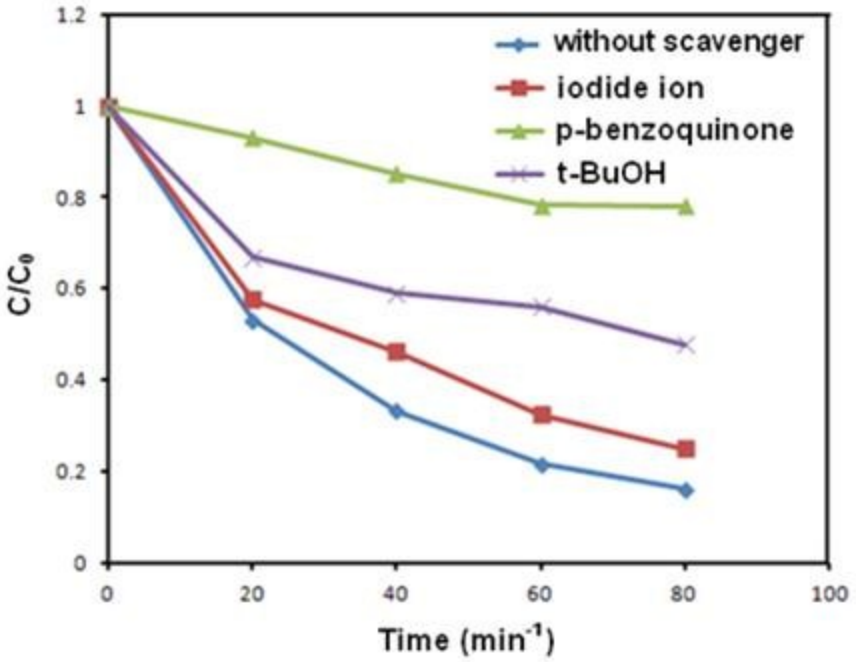

Figure 11. Effect of different scavengers on degradation of AB92 by $Ag_3VO_4/Ag_3PO_4/Ag$.

3. 5. Possible Mechanism

Since $Ag3VO_4$ and Ag_3PO_4 have the band gap energies of 2.2 eV[17] and 2.45 eV[7] respectively, they should be active in visible light region. Photo-induced electrons on the Ag_3VO_4 particles can easily transfer to the surface of Ag_3PO_4 and photo-induced holes of Ag_3PO_4 can also migrate to the surface of the Ag_3VO_4. These transformation are due to the fact that the CB and VB of Ag_3VO_4 (CB = 0.04 eV, VB = 2.24 eV)[17] are more negative than that of Ag_3PO_4 (CB = 0.45 eV, VB = 2.87 eV).[12] Therefore, the efficiency of the photo-induced charge-separation process was enhanced, and more charge carriers can increase the degradation of AB92. When Ag NPs was deposited on the surface of the Ag_3VO_4/Ag_3PO_4 composite, enhancement of photocatalytic activity was observed. Under visible light irradiation, Ag NPs act as electron acceptors, and

electrons on the CB of the Ag_3PO_4 can be easily transferred into Ag NPs because CB of Ag_3PO_4 is more negative than the Fermi level of deposited Ag NPs through the Schottky barrier.[29-30]

The CB level of Ag_3PO_4 is more negative than the standard redox potential of O_2/H_2O_2 (0.682 eV vs. NHE), [31] hence, electrons on the surface of Ag_3PO_4 can be trapped by molecular oxygen in the solution to form H_2O_2. H_2O_2 in turn reacts with electrons to produce active $OH^{\bullet}$ in solution, and subsequently, these active radical get involved in photocatalytic degradation of AB92. However, the standard redox potential of $O_2/O_2^{\bullet-}$ (-0.33 eV vs. NHE) [32] is so negative that electrons in the CB of Ag_3PO_4 cannot reduce O_2 to $O_2^{\bullet-}$ or $HO_2^{\bullet}$. Upon visible light irradiation photo-exited electrons in Ag_3PO_4 are transferred to Ag NPs. This accumulated electrons in the Ag NPs react whit O_2 molecules to produce $O_2^{\bullet-}$.[33-34] The VB position of Ag_3VO_4 is less positive than the standard redox potential of $OH^{\bullet}$, H^+/H_2O (2.72 eV vs. NHE),[35] suggesting that the accumulated holes in the VB of Ag_3VO_4 cannot oxidize H_2O to form adsorbed $OH^{\bullet}$ [17] while they can oxidize OH^- to form $OH^{\bullet}$ in solution because the VB of Ag_3VO_4 is more positive than the standard redox potential of $OH^{\bullet}/OH^-$ (1.99 eV vs. NHE).[36] These enriched holes on the VB of Ag_3VO_4 can also directly decompose the absorbed AB92 on the surface of the catalysts. Based on the above results and the mentioned discussion, the possible photocatalytic mechanism of the $Ag_3VO_4/Ag_3PO_4/Ag$ can be proposed as shown in Scheme. 1.

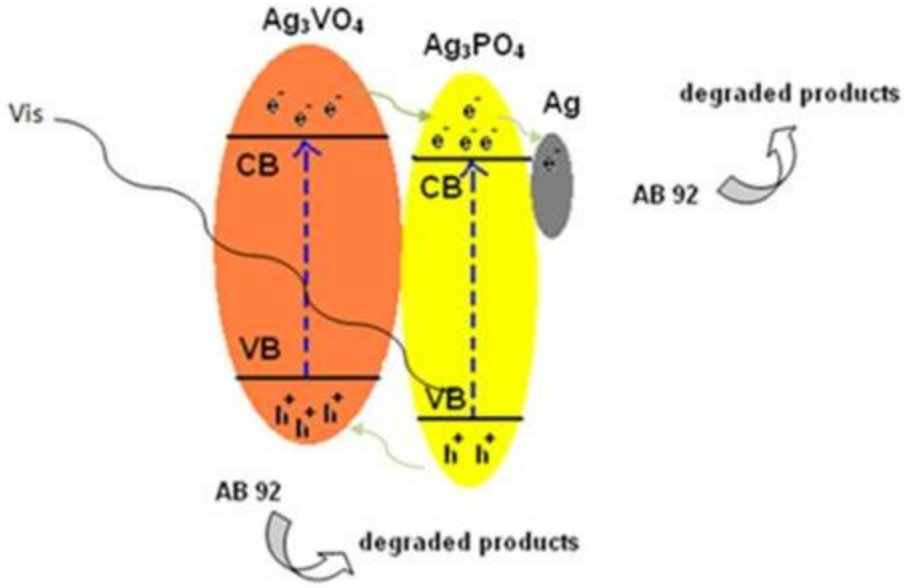

Scheme 1. Schematic illustration of photocatalytic mechanism and charge transfer of the $Ag_3VO_4/Ag_3PO_4/Ag$ under visible light irradiation.

Under visible light irradiation, both Ag_3VO_4 and Ag_3PO_4 can be exited. Photo-induced electrons in the CB of the Ag_3VO_4 can be transferred to that of Ag_3PO_4. These electrons can be trapped by molecular oxygen in solution to form $OH^{\bullet}$ and other oxidative species or migrate to the surface of Ag NPs and then participate in photocatalytic reactions. Photo-induced holes in the VB of Ag_3PO_4 can migrate to the surface of Ag_3VO_4 and can directly oxidize the adsorbed dye on the surface of the catalysts.

4. Conclusion

Novel visible-light-driven $Ag_3VO_4/Ag_3PO_4/Ag$ photocatalyst has been successfully prepared via an in situ anion-exchange process, followed by light reduction. The $Ag_3VO_4/Ag_3PO_4/Ag$

nanocomposite show much higher photocatalytic activity than Ag_3VO_4/Ag_3PO_4 heterocatalyst and pure Ag_3VO_4 for degradation of AB92 under visible light irradiation. Photocatalytic activity of Ag_3VO_4 increased with coupling by Ag_3PO_4, due to improving the transfer of photo-induced electron-hole pairs between Ag_3PO_4 and Ag_3VO_4. Furthermore, Ag NPs promote migration efficiency of the photogenerated electrons, and thus enhanced photocatalytic activity of Ag_3VO_4/Ag_3PO_4.

References

1. A. Fujishima and K. Honda, *Nature*, 1972, **238**, 37-38.

2. X. Zhang, L. Zhang, T. Xie and D. Wang, *J. Phys. Chem. C*, 2009, **113**, 7371-7378.

3. H. Wang, L. Zhang, Z. Chen, J. Hu, S. Li, Z. Wang, J. Liu, X. Wang, *Chem. Soc. Rev*., 2014, **43**, 5234-5244.

4. N. Wetchakun, S. Chaiwichain, B. Inceesungvorn, K. Pingmuang, S. Phanichphant, A. I. Minett, J. Chen, *ACS Appl. Mater. Interfaces*, 2012, **4**, 3718-3723.

5. H. Dong, G. Chen, J. Sun, C. Li, Y. Yu and D. Chen, *Appl. Catal,. B*, 2013, **134-135**, 46-54.

6. W. Zhou, H. Liu, J. Wang, D. Liu, G. Du and J. Cui, *ACS Appl. Mater. Interfaces*, 2010, **2(8)**, 2385-2392.

7. P. Wang, P. Shi, Y. Hong, X. Zhou and W. Yao, *Mater. Res. Bulletin*, 2015, **62**, 24-29.

8. H. Yu, L. Liu, X. Wang, P. Wang, J. Yu and Y. Wang, *Dalton. Trans*, 2012, **41**, 10405-10411.

9. B. Tian, T. Wang, R. Dong, S. Bao, F. Yang and J. Zhang, *Appl. Catal., B*, 2014, **147**, 22-28.

10. L. Sun, R. Zhang, Y. Wang and W. Chen, *ACS Appl. Mater. Interfaces*, 2014, **6(17)**, 14819-14826.

11. M. Long and W. Cai, *Nanoscale*, 2014, **6**, 7730.

12. Z. Chen, W. Wang, Z. Zhang and X. Fang, *J. Phys. Chem. C*, 2013, **117**, 19346-19352.

13. H. Xu, J. Zhu, Y. Song, W. Zhao, Y. Xu, Y. Song, H. Ji and H. Li, *RSC Adv*, 2014, **4**, 9139-9147.

14. W. Wang, H. Du, R. Wang, T. Wen and A. Xu, *Nanoscale*, 2013, **5**, 3315-3321.

15. Q. Zhu, W. Wang, L. Lin, G. Gao, H. Guo, H. Du and A. Xu, *J. Phys. Chem. C*, 2013, **117**, 5894-5900.

16. R. Konta, H. Kato, H. Kobayashi and A. Kudo, *Phys. Chem. Chem. Phys.*, 2003, **5**, 3061-3065.

17. S. Wang, D. Li, C. Sun, S. Yang, Y. Guan and H. He, *Appl. Catal. B*, 2014, **144**, 885-892.

18. S. Wang, Y. Guan, L. Wang, W. Zhao, H. He, J. Xiao, S. Yang and C. Sun, *Appl. Catal. B*, 2015, **168**, 448-457.

19. L. Zhang, Y. He, P. Ye, Y. Wu and T. Wu, *J. Alloys Compd*, 2013, **549**, 105-113.

20. Z. Yang, G. Huang, Wei Huang, J. Wei, X. Yan, Y. Liu, C. Jiao, Z. Wan and A. Pan, *J. Mater. Chem. A*, 2013, **2**, 1750-1756.

21. C. Shifu, Z. Wei, L. Wei, Z. Huaye, Y. Xiaoling and C. Yinghao, *J. Hazard. Mater*, 2009, **172**, 1415-1423.

22. N. Tian, H. Huang, Y. He, Y. Guo, T. Zhang and Y. Zhang, *Dalton Trans*, 2015, **44**, 4297-4307.

23. N. Mohaghegh, E. Rahimi and M.R. Gholami, *Mater. Sci. Semicond. Process.*, 2015, **39**, 506-514.

24. Y.Sang, Y. Huang, W. Wang, Z. Fang and B. Geng, RSC Adv., 2015, **5**, 39651-39656.

25. H. Cheng, B. Huang, P. Wang, Z. Wang, Z. Lou, J. Wang, X. Qin, X. Zhang and Y. Dai, Chem. Comm., 2011, **47**, 7054-7056

26. Z. He, Y. She, C. Gao, L. Wen, J. Chen and S.Song, *J. Phys. Chem. C*, 2014, **118**, 389-398

27. D. D. Zhang, R. L. Qui, L. Song, B. Eric, Y. Q. Mo and X. F. Huang, *J. Hazard. Mater*, 2009, **163**, 843- 847

28. I. K. Konstantinou and T. A. Albanis, *Appl. Catal. B*, 2004, **49**, 1-14.

29. Z. Cheng, F. Bing, Q. Liu, Z. Zhang and X. Fang, *J. Mater. Chem A.*, 2014, **00**, 1-3.

30. H. Katsumata, T. Sakai, T. Suzuki and S. Kaneco, *Ind. Eng. Chem. Res*. 2014, **53**, 8018-8025.

31. M. Antoniadou and P. Lianos, *Appl. Catal. B*, 2010, **99**, 307-313.

32. W. Liu, M. Wang, C. Xu, S. Chen and X. Fu, *Mater. Res. Bull*, 2013, **48(1)**, 106-113.

33. H. Hu, Z. Jiao, T. Wang, J. Ye, G. Lu and Y. Bi, *J. Mater. Chem. A*, 2013, **1**, 10612-10616.

34. J. Xiong, Z. Li, J. Chen, S. Zhang, L. Wang and S. Dou, *ACS Appl. Mater. Interfaces*, 2014, **6 (18)**, 15716–15725.

35. G. Li, K.H. Wong, X. Zhang, C. Hu, J.C. Yu, R.C.Y. Chan and P.K. Wong, *Chemosphere*, 2009, **76**, 1185-1191.

36. M. Xu, L. Han and S. Dong, *ACS* Appl. Mater. *Interfaces*, 2013, **5**, 12533-12540.

Coreesponding email:

(*Corresponding author e-mail: Setayesh@sharif.edu)

(*Corresponding author e-mail: gholami@sharif.edu)

Acknowledgment:

Authors would like to express their special thanks to Dr. Mohammad Mahdi Ahadian for his kind supports.

Table of Content

The novel $Ag_3VO_4/Ag_3PO_4/Ag$ photocatalyst with enhanced photocatalytic activity.